THE INTERNATIONAL JOURNAL OF SCIENCE & TECHNOLEDGE

Synthesis, Spectral Characterization and Study of Electronic Properties of 5-(3,5-Difluoro-4-Hydroxy Phenyl)- 5,6,7,8-Tetrahydro-7-Thioxopyrimido [4,5-D]-Pyrimidine-2,4 (1h,3h)-Dione Using Density Functional Theory

D. Durga Devi
Research Scholar, PG & Research, Department of Chemistry,
Government Arts College, Chidambaram, Tamil Nadu, India
Dr. S. Manivarman
Assistant Professor, PG & Research, Department of Chemistry,
Government Arts College, Chidambaram, Tamil Nadu, India

Abstract:
5-(3,5-difluoro-4-hydroxyphenyl)-5,6,7,8-tetrahydro-7-thioxopyrimido[4,5-d]-pyrimidine-2,4(1H,3H)-dione (DTTP) compound have been synthesized. The structure of the compound was analysed and confirmed by UV, FT-IR, FT-Raman, NMR spectrum. Quantum chemical calculations have been performed to compute molecular structure, atomic charges and electronic properties of the synthesized compound by using DFT/B3LYP/6-31G (d, p) level of theory. The observed and theoretical wave numbers were analysed by means of potential energy distribution. The hyperpolarizability value of the molecule is greater than standard urea, which was also confirmed by frontier molecular orbital analysis. In addition, intra molecular hyperconjugative interactions were analysed by using natural bond orbital analysis.

Keywords: *Pyrimidine, HOMO-LUMO, NLO, NBO, DTTP*

1. Introduction

The chemistry of heterocyclic compounds is the most important in the discovery of new drugs. pyrimidine is one of the most important heterocycles with pharmacological activities because it is an essential constituent of all cells and thus of all living matter [i]. Hence, they have received the consideration of researchers due to its manifold implication viz, antibacterial, antifungal, anticancer, antitumor, antiallergic, analgesic, anti inflammatory, and antineuplastic [ii-iv]. Some pyrimidine derivatives are also reported as good corrosion inhibitors because of the presence of hetero atoms and delocalized π-electrons [v-vii].Generally, nitrogen containing heterocyclic compounds such as pyridine and pyrimidine derivatives favourable for NLO conditions due to the presence of lone pair electrons. Recently pyrimidine derivatives reported as a good non-linear material [viii-x].

In spite of the application of pyrimidine derivatives, a venture has been undertaken for the synthesis of 5-(3,5-difluoro-4-hydroxyphenyl)-5,6,7,8-tetrahydro-7-thioxopyrimido[4,5-d]-pyrimidine-2,4(1H,3H)-dione compound. The aim of present work is to study the structural activity of the DTTP molecule by using density functional theory.

To best of our knowledge, there is no computational studies has been reported for the DTTP compound. Hence, the present investigation deals with using DFT method of calculations along with experimental measurements of FT-IR, FT-Raman spectra was undertaken to study the vibrational spectra of studied molecule completely and to identify the various normal modes with greater wave number accuracy. In this present study, optimized molecular structural parameters, HOMO-LUMO analysis and NLO property (first hyperpolarizability) are carried out to elucidate the information regarding energy gap and charge transfer within the molecule. In addition, molecular electrostatic potential (MEP), mulliken charge distribution and thermodynamic parameters of the DTTP compound are studied by using density functional theory.

2. Computational Details

Density functional theory (DFT) has been proved to be extremely useful in treating electronic structure of the molecules. Gaussian 03 quantum chemical software [xi] was used in all calculations of the DTTP molecule. Optimized structural parameters and vibrational wave numbers for the DTTP molecule were calculated by using B3LYP functional with 6-31G (d, p) basis set. The vibrational modes were assigned on the basis of potential energy distribution analysis using VEDA4 program [xii]. The calculated harmonic vibrational wave numbers were scaled down uniformly by a factor of 0.9608 for B3LYP/6-31G (d, p) level of theory, which accounts for systematic errors caused by basis set incompleteness, neglect of electron correlation and vibrational anhormonicity [xiii-xv].

3. Experimental

3.1. Synthesis of 5-(3,5-difluoro-4-hydroxy phenyl)- 7-thioxo-5,6,7,8-tetrahydropyrimido [4,5-d] -pyrimidine-2,4(1H,3H)-dione

Equal mole ratio (0.003 mol) of barbituric acid, thiourea and 3,5-Difluoro-4-Hydroxy benzaldehyde are dissolved in ethanol then the content is condensed on oil bath for 1 hour in acidic medium. The reaction mixture is poured in water and the product obtained is filtered and dried, finally the product is recrystallized from ethanol. The completion of the reaction was monitored using thin layer chromatography technique.

Yield of the product is 86%

Melting point of the product is 184° C.

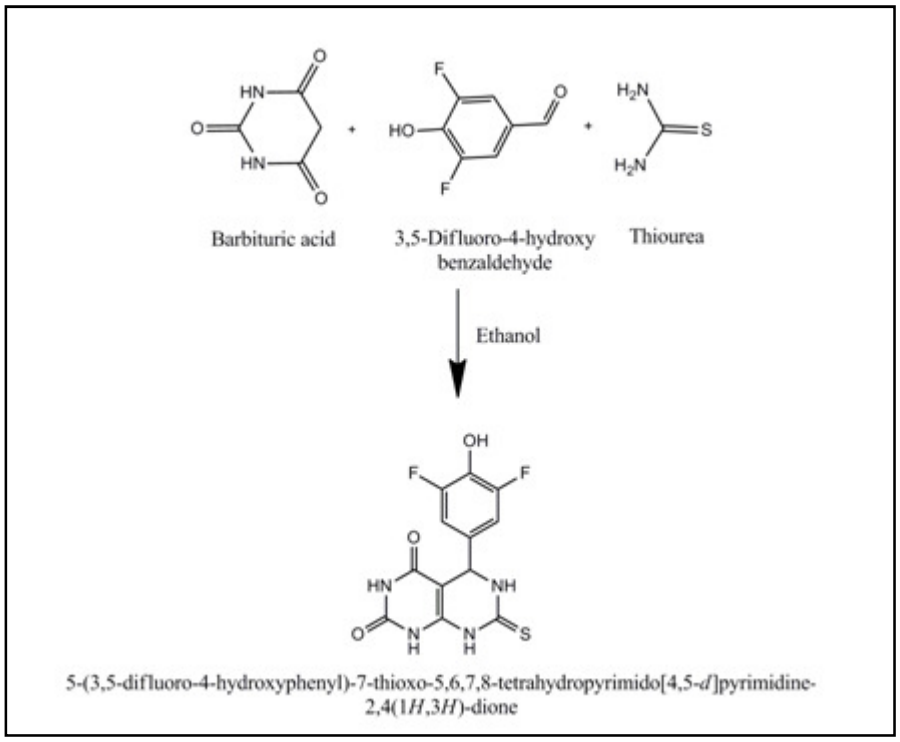

Figure 1

4. Results and Discussion

→ Structural determination by IR and NMR spectra of 5-(3,5-difluoro-4-hydroxy phenyl)- 7-thioxo-5,6,7,8-tetrahydropyrimido [4,5-d] -pyrimidine-2,4(1H,3H)-dione

^{1}H NMR (400 MHz, $DMSOD_6$): δ= 5.20 (s, 1H, ArCH), 6.27-7.36 (m, 5H, ArH), 9.37 (s, 1H, NH), 9.53 (s, 1H, NH), 9.83 (s, 1H, NH), 10.91 (s, 1H, NH). 5.56 (s, 1H, OH),^{13}C NMR (75 MHz, $DMSOD_6$): δ =165.84, 170.17, 189.13, 82.84, 45.19, 125.31-160.41; IR (KBR) νcm^{-1} = 3365, 3265, 3174 cm^{-1} (NH), 2964 cm^{-1} (CH–Aromatic), 1697 cm^{-1} (C=O), 1523 cm^{-1} (CONH).

4.1. Molecular Geometry

The optimized molecular structure of the DTTP molecule along with the numbering scheme of the atoms obtained from Gauss View program is shown in Fig. 1. The structural parameters of DTTP are shown in Table 1. To the best of our knowledge, no X-ray crystallographic data of the title compound has been reported. However, the theoretical results are compared with the reported structural parameters of analogous molecules.

The C–C bond length in the title compound lies within the range of 1.36–1.40 Å. The linkage formed between phenyl ring and pyrimidine ring at the position of C_3–C_9 is slightly higher, due to presence of Sp^3 hybridized carbon atom (C_9). In pyrimidine ring, the bond distance of C_3–C_4 is calculated as 1.36 Å, while this value lower than the bond length of C_2–C_3, C_3–C_9, which indicate the double bond character of C_3–C_4 bond and is correlated with *shilka et.al.*[xvi]. The C–F (1.35 Å) and C–N (1.35-1.41 Å) bond length values are in good agreement with the crystal data of analogous molecule with exception of C_9–N_{14} which is positively (0.06 Å) deviated from *krishnamurthyet.al* [xvii].

Typically, SP^2 hybridized carbon atom shows their bond angle around 120°[xviii]. In DTTP molecule, the calculated C_{20}–C_{18}–C_{17}, C_{18}–C_{17}–C_{19}, C_{17}–C_{19}–C_{22} bond angles (118°, 119° and 120°) are in line with *dwivedi et.al* [xix].However, C_{18}–C_{20}–C_{24}, C_{20}–C_{24}–C_{22}, C_{24}–C_{22}–C_{19} bond angles are considerably deviated. This is due to, the substitution of electron withdrawing nature of halogen and electron donating nature of hydroxyl groups and their bond angles are 123°, 116°, 121°. In addition, C–C–C bond angle in pyrimidine are around 120° and C–N–C, N–C–N, C–N–H bond angles of pyrimidine are listed in Table 1.

4.2. Vibrational Assignments

The molecule DTTP 30 atoms; hence one can have 84 normal modes of vibrations. The title molecule DTTP belongs to C_1 point group symmetry. The recorded FT-IR, FT-Raman and calculated wave number, intensities, force constant, reduced mass are given in Table S1. The comparisons of experimental and theoretical spectra are shown in Fig. 2 (FT-IR) and Fig. 3(FT-Raman).

4.2.1. C–H Vibrations

Aromatic C–H stretching vibrations, commonly exhibit multiple weak bands in the region of 3100-3000 cm^{-1}[xx-xxii]. In the present study, the band observed at 3069 cm^{-1} in FT-IR spectrum assigned to C–H stretching vibration and the calculated wave number observed at 3097 cm^{-1}. This vibrational mode is a pure stretching mode with 100% of PED contribution, as it is evident from Table S1. The aromatic C–H in-plane-bending and out-of-plane bending vibrations observed at 1300-1000 cm^{-1} and 900-690 cm^{-1} respectively [xxiii, xxiv]. Experimentally the band observed at 1194 cm^{-1} in FT-Raman is assigned to in-plane-bending vibration of C–H bond. Weak band observed at 862 cm^{-1} in FT-IR and 813 cm^{-1} FT-Raman spectrum are assigned to out-of-plane bending vibration of aromatic C–H bond. The calculated deformation observed at 1192, 835, 852 cm^{-1}. The aliphatic C–H stretching vibration appeared at 2964 cm^{-1} in FT-IR spectrum and this wave number show good agreement with theoretical wave number at 2947 cm^{-1}.

4.2.2. C–C Vibration

The aromatic ring carbon–carbon stretching modes appear in the region of 1650-1200 cm^{-1}[xxv]. In general, the bands are of variable intensity and are observed at 1625-1590, 1575-1590, 1470-1540, 1430-1465 and 1280-1380 cm^{-1} for five bands in the region given by Varsanyi [xxvi]. Most of the ring modes are altered by the substitution to aromatic ring [xxvii].

In the present study, the band observed at 1616 cm^{-1}(FT-IR) is assigned to C–C stretching vibration of the DTTP molecule and the theoretical wave number show excellent correlation with observed wave number at 1614 cm^{-1}. The C–C–C in-plane-bending vibration observed as a weak band in FT-IR at 486 cm^{-1} and FT-Raman spectrum at 478 cm^{-1}. These vibrations show good agreement with theoretical wave number at 477 cm^{-1}. In pyrimidine ring, the stretching vibration of $\nu(C_3{=}C_4)$ has been calculated at 1639 cm^{-1} with 62% of PED contribution and this band observed in FT-Raman spectra at 1619 cm^{-1}.

4.2.3. O–H Vibration

Non-hydrogen bonded or free hydroxyl group gives peaks at the rangeof 3550-3700 cm^{-1}[xxviii, xxix]. In the present study, the O–H stretching frequency experimentally observed at 3734 cm^{-1} in FT-IR spectrum and the O–H in-plane-bending vibration observed at 1226 cm^{-1} in FT-Raman spectrum. This value exactly correlates with theoretical wave number at 1224 cm^{-1}. The band appeared at 399 cm^{-1} in FT-Raman spectrum is assigned to out-of-plane bending of O–H bond and the frequency in line with the calculated wavenumber at 409 cm^{-1}. *Balachandran et.al* [xxx], assigned the bands at 1192 and 384 cm^{-1} for deformation vibration of hydroxyl group.

Generally, the C–O stretching vibration occurs as a strongest band in the region 1300-1200 cm^{-1}[xxxi]. In the present study, the νC_{24}–O_{27} stretching vibration observed at 1244 cm^{-1} in FT-Raman spectrum and is computed at 1248 cm^{-1}.

4.2.4. C=O Vibration

The carbonyl group vibrations give rise to characteristic bands in the vibrational spectra. In the present case the stretching mode of C=O is assigned at 1697 cm^{-1} in FT-IR spectrum and 1767, 1680 cm^{-1} in FT-Raman spectrum. These values computed at 1704 and 1778 cm^{-1}. The deformation modes of carbonyl group observed at 719 cm^{-1} in FT-IR and 733 cm^{-1} in FT-Raman spectrum and these vibrations show good agreement with calculated values at 712 and 730 cm^{-1}. *Pawlukojc et.al*[xxxii], assigned 1786 cm^{-1} for stretching vibration and 723 cm^{-1} for deformation vibration of carbonyl group.

4.2.5. N–H Vibration

The N–H stretching vibrations generally occur in the region of 3500-3000 cm^{-1}. The FT-IR bands appeared at 3365 and 3265 cm^{-1} has been assigned to N–H stretching vibration of the DTTP molecule and the computed wavenumbers observed at 3495, 3491, 3485 and 3482 cm^{-1}.

In C–N–H vibration, the nitrogen and hydrogen move in contrary directions, subsequently, the relative carbon atom involve both N–H bend and C–N stretching vibration, absorbs near 1500 cm^{-1}. Similarly, where the N and H atoms move in the same direction relative to the carbon atom give rise to a weaker band near 1250 cm^{-1}[xxxiii]. In the present study, the bands observed at 1523, 1400, 1334 cm^{-1} in FT-IR spectrum and 1336 cm^{-1}in FT-Raman spectrum is assigned to N–H deformation vibration. These wave numbers show good agreement with computed values 1533, 1403 and 1339 cm^{-1} at mode no. 14, 18 and 22 with maximum 65% of PED contribution and also these wave numbers in line with the literature at 1378 cm^{-1} reported by *sebastian et.al* [xxxiv].

4.2.6. C–N Vibration

The C–N vibration is always mixed with other bands and usually occurs in the region 1382-1266 cm^{-1}[xxxv, xxxvi]. In the present study the C–N stretching is observed at 1072 cm^{-1} in FT-IR and 1383, 1092 cm^{-1} in FT-Raman spectrum. These vibrations show better agreement with calculated wave number at 1080 and 1378 cm^{-1}.

4.2.7. C=S Vibration

In nitrogen containing thiocarbonyl compounds, the assignment of the C=S stretching frequency has been controversial one [xxxvii, xxxviii]. In this study, C=S stretching mode observed at 1126 cm^{-1} in FT-IR spectra and this value in accordance with theoretically calculated value at 1108 cm^{-1}. *Sathyanarayana et al* [xxxix],observed the absorption at 1140 cm^{-1} is being due to C=S stretching of pyrimidine-2-thione. In addition, in-plane-bending vibration of thiocarbonyl group has been calculated at 261 cm^{-1} and the value coincides with the experimental value at 269 cm^{-1}.

4.3. Molecular Electrostatic Potential

The electrophilic and nucleophilic charge sites of DTTP compound can be predicted by molecular electrostatic potential surface and is shown in Fig.4. In DTTP molecule, the oxygen atom in carbonyl group is surrounded by a greater surface of negative charge (red colour) becoming this site potentially more favourable for electrophilic attack. The positive potential (blue colour) located at site of hydrogen atom bonded with nitrogen in pyrimidine ring and fluorine atom. The green colour represents the neutral region of DTTP molecule.

4.4. Mulliken Charge Distribution

Atomic charges directly related to the chemical bonds and vibrational properties hence it affects dipole moment and polarizabilities [xl]. The illustration of mulliken atomic charges are plotted in Fig. 5 and listed in Table 2.

The result shows that, the charge at sites of the C atom attached to the N, O and F atoms are positive. Because of the electron donating nature of the N, O, F atoms and the carbon attached with hydrogen atom shows negative charge. Furthermore, C_6 atom has higher positive charge in atomic distribution owing to its bonding with neighbouring electronegative O and N in its adjacent position. The entire electronegative atoms of DTTP compound show negative charge. In which N_5 atom shows more electro negative charge (-0.658) than residual atoms.

4.5. Frontier Molecular Orbitals

The FMOs plays an important role in the optical and electrical properties, as well as in quantum chemistry [xli].A molecule having a small frontier orbitals gap is more polarizable and is normally related to a high chemical reactivity and low kinetics stability [xlii- xliv].

In the present study, the HOMO-LUMO energies and their energy gap of the title compound are shown in Fig. 6 and found that the lower energy gap ΔE = 4.5117 eV, it indicates the molecule is highly reactive. As can be seen from the figure, LUMO is delocalized among all the atoms of the compound. By contrast, HOMO is located over thio carbonyl moiety of DTTP molecule, hence, electron delocalization mainly takes place in thiocarbonyl moiety and is also evident from enormous stabilization energy of C=S from NBO analysis. Frontier molecular orbital values of DTTP molecule is presented in Table 3.

Conceptual DFT based descriptors have helped in many ways to understand the structure of molecules and their reactivity by calculating the chemical potential, global hardness and electrophilicity index [xlv - xlvii] and their values are listed in Table. 4. Furthermore, the chemical potential of the title compound is negative and it means that the DTTP compound is stable.

DOS spectrum represents the number of energy level on the energy axis that the section has width dE and the spectrum is convoluted with Gaussian curves of heights equal to the calculated contributions for each orbital. The most important application of the DOS plot is to demonstrate MO (Molecular orbital) compositions and their contribution to chemical bonding [xlviii].Dos spectrum of DTTP is shown in Fig. S1.

4.6. Electronic Absorption Spectra

The electronic absorption spectra of the title compound in ethanol solvent were recorded in the 200 - 600 nm range and representative spectrum is shown in Fig. S2. As can be seen from the figure, the experimental electronic absorption spectra of the title compound show two bands, one at 466 nm with log ε = 0.127 and another one at 235 nm with log ε = 3.645. Electronic absorption spectra of the title compound were calculated using the TD-DFT method based on the B3LYP/6-31G (d, p) level optimized structure in gas phase are shown Table S2.

The theoretical absorption bands are predicted at 345, 307, 283 nm and can easily be seen that the absorption at 283 nm correspond to the experimental absorption ones and absorption band have slight red-shift with value 48 nm and is assigned for π-π^* transition. The theoretical and experimental UV-Vis spectrum is shown in Fig.S2.

4.7. Non-Linear Optics

NLO studies are a key technique in the field of telecommunication, signal processing and optical instrumentations, which use light instead of electron for data transition. Polarizability and hyperpolarizability are important quantities to determine the NLO property of a system [xlix-liii]. In order to investigate the NLO property of the DTTP molecule, polarizability and hyperpolarizability was calculated by using B3LYP/6-31G (d, p) level of theory by finite filed approach.

Urea is one of the prototypical molecules used in the study of the NLO properties of molecular systems. Therefore, it was used frequently as a threshold value for comparative purposes. The calculated values of μ, α and $\beta_0$for the DTTP compound are 0.5487 Debye, 0.4241×10^{-30}esu and 6.637×10^{-30} esu, which are greater than those of urea (the $\mu$and $\beta_0$of urea are 1.3732 Debye and 0.3728×10^{-30}esu obtained by B3LYP/6-31G (d, p) method). Theoretically, the first hyperpolarizability of the DTTP compound is seventeen times greater than that of urea. According to the magnitude of the first hyperpolarizability, the title compound may be a potential applicant in the development of NLO materials.

The NLO responses can be understood by means of investigating the frontier molecular orbitals calculations. It is found that there is an inverse relation between hyperpolarizability and the energy gap. Larger value of molecular polarizability is due to smaller value of HOMO-LUMO gap which increase charge transfer [liv-lvi]. From the Table 5, the present study reveals that the energy gap (ΔE) of studied molecule is calculated to be 4.5117 eV, which is lower than urea 7.6644 eV [10]. This result indicated that, the title compound is a suitable aspirant for NLO activity.

4.8. Natural Bond Orbital Analysis

The NBO analysis has been used to understand the intramolecular hydrogen bonding, intramolecular charge transfer (ICT) interaction and the interaction among the bonds. The hyperconjugative interaction energy can be deduced from second-order perturbation approach. The stabilization energy $E^{(2)}$ associated with the delocalization i→j, which is estimated for each donor (i) and acceptor (j) by using the following equation,

$$E^{(2)}=\Delta E_{ij}=q_i\frac{F(i,j)^2}{\varepsilon_j-\varepsilon_i} \quad (1)$$

Where q_i is the donor orbital occupancy, are ε_i and ε_j diagonal elements and F(i, j) is the off diagonal NBO Fock matrix element [lvii]. The intra molecular interactions are formed by the overlap between bonding and anti-bonding orbitals of C=C, C=O, C=S which results in intra molecular charge transfer causing stabilization of DTTP molecule. The electron densities of donor and acceptor orbitals, types of interaction and their respective stabilization energies are listed in Table S3.

In the present study, the σ bonds have higher electron density than the π bonds, hence σ– σ* interaction have minimum delocalization energy then π– π* interaction. The highest electron density of σ bond is 1.9947e, which occurs in donor orbital of $\sigma(C_{20}–F_{25})$ conjugate with acceptor $\sigma^*(C_{17}–C_{18}, C_{22}–C_{24})$ anti-bonding orbital and this interaction weaken their bonds. Considering π-π* interaction, the lowest electron density of 1.6378 observed in donor $\pi(C_{22}–C_{24})$ orbital delocalized with moderate energy of 82.68 and 87.91 kJmol^{-1} to their anti-bonding orbitals $C_{17}–C_{19}$ and $C_{18}–C_{20}$ respectively and this intra molecular charge transfer clearly shows elongation of respective bonds. Similar interaction has been takes place in $\pi(C_{18}–C_{20})\rightarrow \pi^*(C_{17}–C_{19}, C_{22}–C_{24})$ with stabilization energy of 78.74 and 81.34 kJmol^{-1}.

The lone pair electrons are readily available for the interaction with excited electrons of acceptor anti-bonding orbital. During n-π* interaction, more energy delocalization takes place. It is evident from the table, the intra molecular conjugative interaction takes place from lone pair orbital of N_1 to anti-bonding $\pi^*(C_2–O_8, C_6–O_{12})$ with maximum energy of 214.85 and 265.27 kJmol^{-1} which leads to strong stabilization in pyrimidine ring. Furthermore, N_5 and O_{27} stabilize the energy of 196.48, 214.18 and 121.71 kJmol^{-1} with their respective anti-bonding orbitals ($C_3–C_4$, $C_6–O_{12}$, $C_{22}–C_{24}$).

4.9. Thermodynamic Properties

The values of some of the thermodynamic parameters such as specific heat capacity, entropy and enthalpy of the TMTPD compound can be calculated by B3LYP method from 100K to 1000K at 1 atm pressure. The thermodynamic functions are increasing with increase in temperature which may be due to the fact that molecular vibrational intensities increase with temperature [lviii]. The same characteristics are also observed in the present study and the values are presented in Table S4. The quantum computational methods have to be refined more with correlation to elucidate closer approximate values of thermodynamic parameters shown in Fig. 7 and their fitting factor R^2 of entropy, heat capacity and enthalpy are 0.9578, 0.9683 and 0.9996 respectively.

These thermodynamic data can be used to compute other thermodynamic functions to determine the direction of chemical reactions according to the law of thermodynamic [lix].

5. Conclusion

The DTTP compound has been synthesized via Biginelli condensation method. The structure was determined and characterized by FT-IR, FT-Raman, NMR and UV analysis. The main focus of our study is to analyse complete vibrational and molecular structure of DTTP compound. The complete vibrational assignments of wave numbers are made on the basis of potential energy distribution. The close agreements between the experimental and scaled frequencies were achieved. The calculated first hyperpolarizability is found to be 6.637×10^{-30}*esu*, which is seventeen times greater than urea and the energy gap between Homo-Lumo is found to be 4.5117 eV, hence the DTTP molecule is highly reactive. Higher the polarizability value and lowering of ΔE value indicate that charge transfer interaction taking place within the molecule. Reactive sites and charge of the each atom were identified by MEP and mulliken population analysis. The absorption analysis found that π-π* transition mainly takes place in DTTP compound.

6. References

i. Sasada, T. Kobayashi, F. Sakai, N. Konakahara, T. (2009) "An unprecedented approach to 4,5-disubstituted pyrimidine derivatives by a $ZnCl_2$-catalyzed three-component coupling reaction", Org. Lett., 11, 2161-2164.

ii. Goyal, R. D. Prakash, L. (1992) "synthesis of 5,7-disubstituted pyrido2,3-d-pyrimidine derivatives and their antibacterial activity", Indian J. Chem., 31B, 719-720.

iii. Rahaman, A. Hafez, H. N. (2009) "Synthesis of 4-substituted pyrido[2,3-d]pyrimidin-4(1H)-one as analgesic and anti-inflammatory agents", Bioorg. Med. Chem., 19, 3392–3397.

iv. Huang, H. Hutta, D. A. Des jarlais, R. L. Schubert, C. Petrounia, L. P. Chaikin, M. A. Manthey, C. L. Player, M. R. (2008) "Design and synthesis of a pyrido[2,3-d]pyrimidin-5-one class of anti-inflammatory FMS inhibitors", Bioorg. Med. Chem. Lett., 18, 2355–2361.

v. Elewady, G. Y. (2008) "Pyrimidine Derivatives as Corrosion Inhibitors for Carbon-Steel in 2M Hydrochloric Acid Solution", Int. J. Electrochem. Sci,. 3, 1149–1161.

vi. Caliskan, N. Akbas, E. (2012) "Corrosion inhibition of austenitic stainless steel by some pyrimidine compounds in hydrochloric acid", Mater. Corros., 63, 231–237.

vii. Li, X. H. Xie, X. G. (2013) "Inhibition Effect of Pyrimidine Derivatives on the Corrosion of Steel in Hydrochloric Acid Solution", Acta Phys. Chim. Sin., 29, 2221–2231.

viii. Balakrishnan, V. Andavan, P. M. (2012) "Scaled quantum chemical studies of the structure, vibrational spectra and first order hyperpolarizability of 2-amino-4-pyrimidinol", Elixir. Comp. Chem., 44, 7425-7429.

ix. Assam Barakat et.al., (2015) "Synthesis and molecular characterization of 5,5'-((2,4-dichlorophenyl)methylene)bis(1,3-dimethyl pyrimidine-2,4,6(1H,3H,5H)-trione)", J. Mol. Struct., 1084, 207-215,

x. Barakat, A. Al-majid, S. M. (2015) "Synthesis and structure investigation of novel pyrimidine-2,4,6-trione derivatives of highly potential biological activity as anit-diabetic agent", J.mol. struct., 1098, 365-376.

xi. Schlegel, H. B. (1982) "Optimization of equilibrium geometries and transition structures" J. Compt. Chem., 3, 214-218.

xii. Jamroz, M. H., (2004) Vibrational Energy Distribution Analysis, VEDA4 program, Warsaw, Poland.

xiii. Erdogdu, Y. Unsalan, O. Gulluoglu, M. T. (2010) "FT-Raman, FT-IR spectral and DFT studies on 6, 8-dichloroflavone and 6, 8-dibromoflavone", J. Raman Spectrosc., 41, 820-828.

xiv. Erdogdu, Y. Unsalan, O. Amalanathan, M. Hubert joe, J. I. (2010) "Infrared and Raman spectra, vibrational assignment, NBO analysis and DFT calculations of 6-aminoflavone", J. Mol. Struct., 980, 24-30.

xv. Subashchandrabose, S. Krishnan, A. R. Saleem, H. Kavitha, S. Thanikachalam, V. Manikandan, G. (2011) "Synthesis and comparison of bis(4-amino-5-mercapto-1,2,4-triazol-3-yl)butane using DFT study", J. Mol. Struct., 996, 1-11.

xvi. Shelke, A. Karade, N. N. Dutta, P. Kr. Bahekar, S. P. Chandak, H. S. (2015) "Crystal structure, DFT study and Hirshfeld surface analysis of ethyl 5-(3,4-dimethoxyphenyl)-7-methyl-3-phenyl-5H-thiazolo[3,2-a]pyrimidine-6-carboxylate", J. Struct. Chem., 56, 1246-1252.

xvii. Krishnamurthy, M. S. Noor Shahina Begum, (2014) "Crystal structure of ethyl 2-(2-fluorobenzylidene)-5-(4-fluorophenyl)-7-methyl-3-oxo-2,3-dihydro-5H-1,3-thia zolo[3,2-a]pyrimidine-6-carboxylate"Acta Cryst., E70, 1270-1271.

xviii. Kurt, M. Yurdakul, S. (2005) "Molecular structure and vibrational spectra of lepidine and 2-chlorolepidine by density functional theory and ab initio Hartree–Fock Calculations", J. Mol. Struct. Theochem., 730, 59-67.

xix. Dwivedi, A. Siddiqui, S. A. Prasad, O. Sinha, L. Misra, N.(2009) "Quantum chemical calculation 0n 5-phenyl-2-(4-pyridyl)pyrimidine", J. Applied spectroscopy, 76, 5.

xx. Sharma, Y. R. (1994) Elementary Organic Spectroscopy Principles and Chemical Applications, S. Chand & Company Ltd., New Delhi, 92-93.

xxi. Socrates, G. (1997) "Infrared and Raman Characteristic Group Frequencies-Tables and Charts", third Ed., Wiley, Newyork.

xxii. Dollish, F. R. Fateley, W. G. Bentley, F. F. (1974) "Characteristic Raman Frequencies of Organic compounds", Wiley, Newyork.

xxiii. Jamroz, M. H. Dobrowolski, J. Cz. Brzozowksi, R. (2006) "Vibrational modes of 2,6-, 2,7-, and 2,3-diisopropylnaphthalene-A DFT study", J. Mol. Struct., 787, 172-183.

xxiv. Altun, A. Golcuk, K. Kumru, M. (2003) "Structure and vibrational spectra of p-methylaniline, Hartree-Fock, MP2 and density functional theory studies", J. Mol. Struc. (Theochem)., 637, 155-169.

xxv. Arjunan, V. Sakiladevi, S. Marchewka, M. K. Mohan, S. (2013) "FT-IR, FT-Raman, FT-NMR and quantum chemical investigations of 3-acetylcoumarin", Spectrochim. Acta Part A, 109, 79-89.

xxvi. Varsanyi ,G. (1969) Vibrational spectra of Benzene derivatives, Academic Press, New York.

xxvii. Bellamy, L. J. (1959) The Infrared Spectra of Complex molecules, Wiley, Newyork.

xxviii. Teimouri, A. Chermahini, A. N. Taban, K. Dabbagh, H. A. (2009) "Experimental and CIS, TD-DFT, ab initio calculations of visible spectra and the vibrational frequencies of sulfonyl azide-azoic dyes", Spectrochim. Acta A,72(2), 369-377.

xxix. Tamer, O. Sariboga, B. Ucar, I. Buyukgungor, O. (2011) "Spectroscopic characterization, X-ray structure, antimicrobial activity and DFT calculations of novel dipicolinate copper(II) complex with 2,6-pyridinedimethanol", Spectrochim. Acta A, 84(1), 168-177.

xxx. Balachandran, V. Rajeswari, S. Lalitha, S. (2013)"Vibrational spectral analysis, computation of thermodynamic functions for various temperatures and NBO analysis of 2,3,4,5-tetrachlorophenol using ab initio HF and DFT calculations", Spectrochim. Acta Part A, 101, 356-369.

xxxi. Green, J. H. S. Harrison, D. J. Kynaston, W. (1971)"Vibrational spectra of benzene derivatives—XIV, Mono substituted phenols", Spectrochim. Acta, 27, 2199-2217.

xxxii. Pawlukojc, A. Natkaniec, I. Malarski, Z. Leciejewicz, J. (2000) "The dynamical pattern of the 2-aminopyrazine-3-carboxylic acid molecule by inelastic and incoherent neutron scattering, Raman spectroscopy and ab initio calculations", J. Mol. Struc., 516(1), 7-14.

xxxiii. Colthup, N. B. Daly, L. H. Wiberley, S. E. (1964) "Introduction to Infrared and Raman Spectroscopy", Academic press, Newyork.

xxxiv. Sebestian, S. Varghese, H. T. Mary, Y.S. Panicker, C.Y. (2010) "Vibrational spectroscopic and theoretical study of Barbituric acid", Orient. J. chem., 26(3), 1139-1142.

xxxv. Dilella, D. P. Stidham, H. D. (1980) "Vibrational spectra of C_2v deuterium substituted pyridines. 2—Pyridine, pyridine-4-d, pyridine-2,6-d_2 and pyridine-2,4,6-d_3", J. Raman Spectros., 9(2), 90-106.

xxxvi. Udhayakala, P. Boopathi, M. Ramkumaar, G. R. Rajendiran, T. V. Gunasekaran, S. (2015)"Spectroscopic studies and molecular structure investigation on 2-chloro-4-(trifluoromethyl) pyridine, A combined experimental and DFT analysis", Der Pharma Chemica, 7(9), 110-121.

xxxvii. Shanmugam, R. Sathyanarayana, D. " (1984) Raman and polarized infrared spectra of pyridine-2-thione", Spectrochim. Acta A, 40(8), 757-761.

xxxviii. Rao ,C. N. R. (1963) Chemical Applications of Infrared Spectroscopy, Academic Press, Newyork.

xxxix. Sathyanarayana, D. N. Kasmir raja, S. V. (1985) "Molecular vibrations of pyridine-2-thione and pyrimidine-2-thione", Spectrochim. Acta A., 41, 809-813.

xl. Govindarajan, M. Karabacak, M. (2012) "Spectroscopic properties, NLO, HOMO–LUMO and NBO analysis of 2,5-Lutidine"¸ Spectrochim. Acta A, 96, 421-435.

xli. Fleming, L. (1976) Frontier Orbitals and Organic Chemical reactions, John Wiley & Sons, London.

xlii. Sinha, L. Prasad, O. Narayan, V. Shukla, S. R. (2011) "Raman, FT-IR spectroscopic analysis and first-order hyperpolarisability of 3-benzoyl-5-chlorouracil by first principles" J. Mol. Simul., 37(2), 153-163.

xliii. Lewis, D. F. V. Ioannides, C. Parke, D. V. (1994) "Interaction of a series of nitriles with the alcohol-inducible isoform of P450, Computer analysis of structure-activity relationships", Xenobiotica, 24, 401-408.

xliv. Kosar, B. Albayrak, C. (2011) "Spectroscopic investigations and quantum chemical computational study of (E)-4-methoxy-2-[(p-tolylimino)methyl]phenol", Spectrochim. Acta A, 78(1), 160-167.

xlv. Koopmans, T. A. (1934) "Uber die Zuordnung von Wellenfunktionen und Eigenwerten zu den Einzelnen Elektronen Eines Atoms", Physica, 1, 104-113.

xlvi. Parr, R. G. Szentpaly, L. V. Liu, S. (1999) "Electrophilicity Index", J. Am. Chem. Soc., 121(9),1922-1924,1999.

xlvii. Parr, R. G. Pearson, R. G. (1983) "Absolute hardness, companion parameter to absolute electronegativity" J. Am. Chem. Soc., 105(26), 7512-7516.

xlviii. O'Boyle, N. M. (2004) Surface studies and density functional theory analysis of ruthenium polypyridyl complexes, PhD. Thesis, Dublin City University.

xlix. Gubler, U. Concilio, S. Bosshard, C. Biaggio, ., Gunter, P. Martin, R. E, Edelmann, M. J. Wytko, J. A. Diederich, F. (2002) "Third-order non linear optical properties of in-backbone substituted conjugated polymers" Appl. Phys. Lett., 81, 2322-2324.

l. Maroulis, G. (2006) Atoms, Molecules and Clusters in Electric Field, Imperial College Press, London.

li. Bredas, J. L. Adant, C. Tackx, P. Persons, A. Pierce, B. M. (1994) "Third-Order Nonlinear Optical Response in Organic Materials, Theoretical and Experimental Aspects", Chem Rev, 94(1), 243-278.

lii. James, C. Amal Raj, A. Raghunathan, R. Jayakumar, V. S. Hubert Joe, I. (2006) "Structural conformation and vibrational spectroscopic studies of 2,6-bis(p-N,N-dimethyl benzylidene)cyclohexanone using density functional theory", J. Raman Spectrosc., 37(12), 1381-1392.

liii. Liu, J. N. Chen, Z. R. Yuan, S. F. (2005) "Study on the prediction of visible absorption maxima of azobenzene compounds", J. Zhejiang Univ Sci B. 6(6), 584-589.

liv. Akkurt, M. Hokelek, T. Soylu, H. (1987) "Structure of potassium hydrogen L(+)-tartrate, $KH(C_4H_4O_6)$", Zeitschrift fur Kristallographie-Crystalline Materials, 181, 161-165.

lv. Panunto, T. W, Urbanczyk-Lipkowska, Z. Johnson. Etter, M. C. (1987) "Hydrogen-Bond formation in Nitroanilines; The first step in Designing Acentric Materials", J. Am. Chem. Soc., 109(25), 7786-7797, 1987.

lvi. Etter, M. C. Baures, P. W. (1988) "Triphenylphosphine oxide as a crystallization aid", J. Am. Chem. Soc., 110(2), 639-640.

lvii. Chocholousova, J,. Vladimir Spirko, V. Hobza, P. (2004) Phys. Chem. Chem. Phys., 6, 37–41.

lviii. Ott, J. Bevan, J. Boerio-Goates, J. (2000) Calculation from statistical thermodynamics, Academic press.

lix. Zhang, R. Dub, B. Sun, G. Sun, Y. (2010) "Experimental and theoretical studies on o-, m- and p-chlorobenzylideneaminoantipyrines", Spectrochim. Acta, 75A,1115-1124.

Annexure

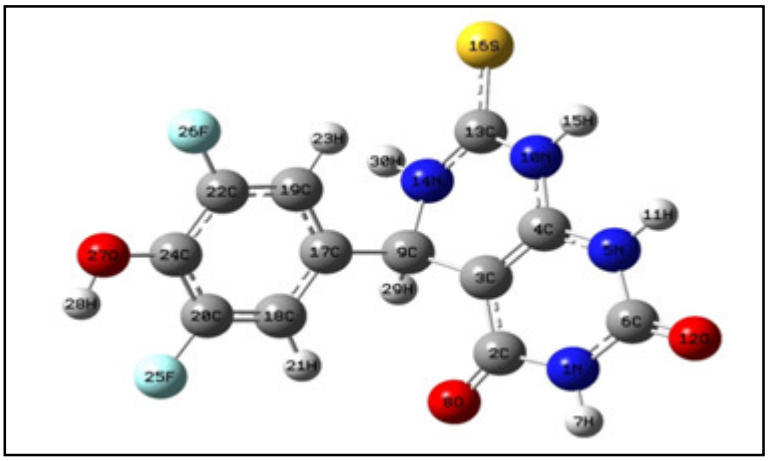

Figure 1: The optimized molecular structure of DTTP

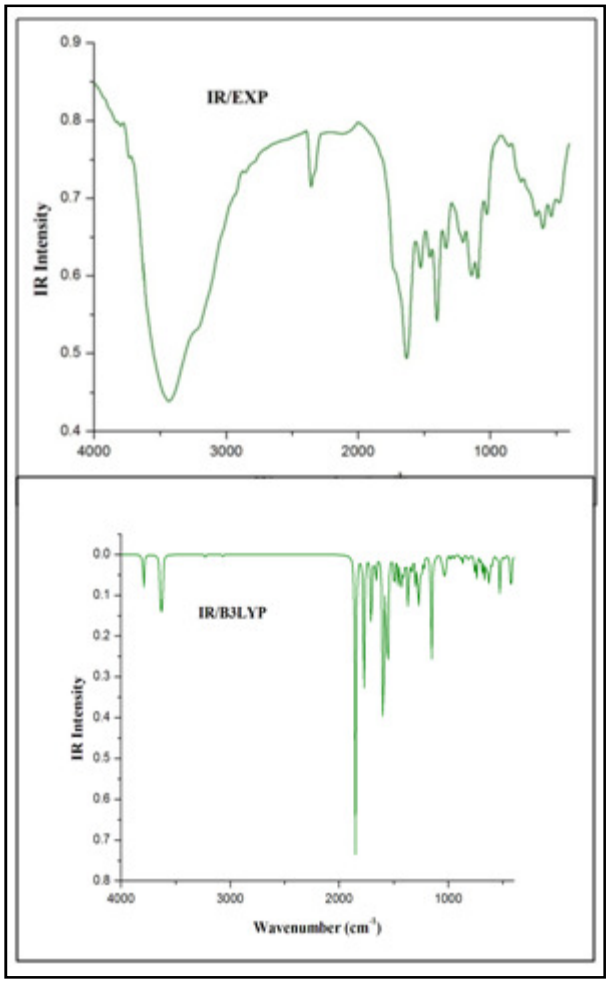

Figure 2: The recorded and simulated IR spectra of DTTP

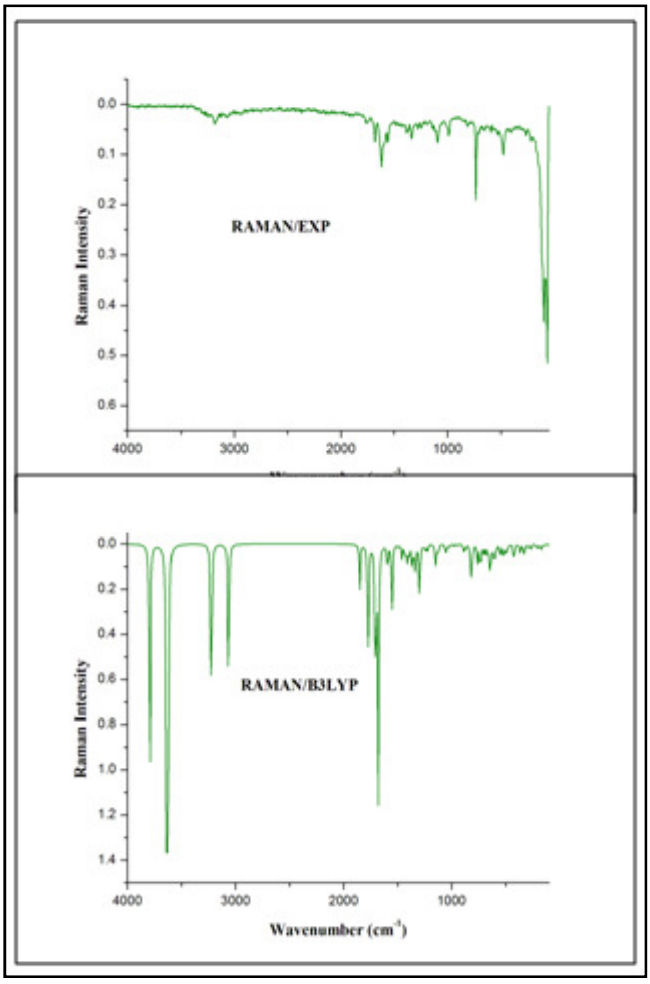

Figure 3: The recorded and simulated Raman specra of DTTP

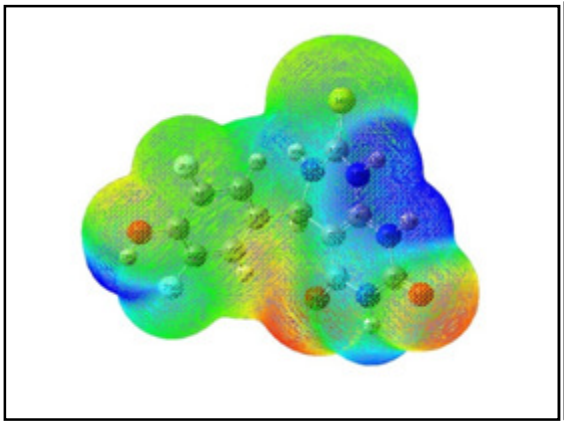

Figure 4: Molecular electrostatic potential of DTTP

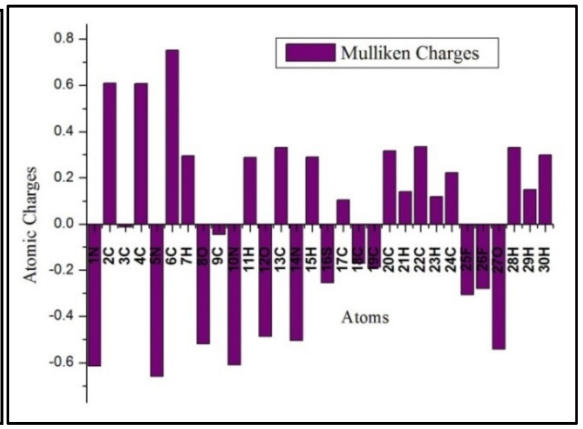

Figure 5: Mulliken atomic charges of DTTP

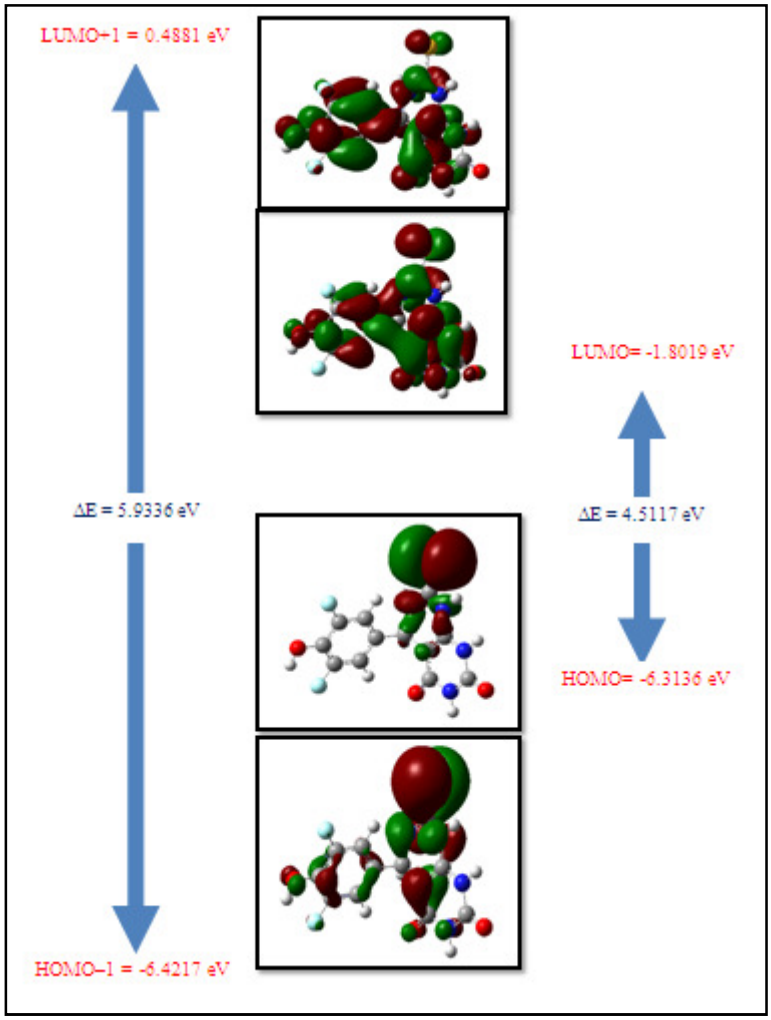

Figure 6: Frontier molecular orbitals of DTTP

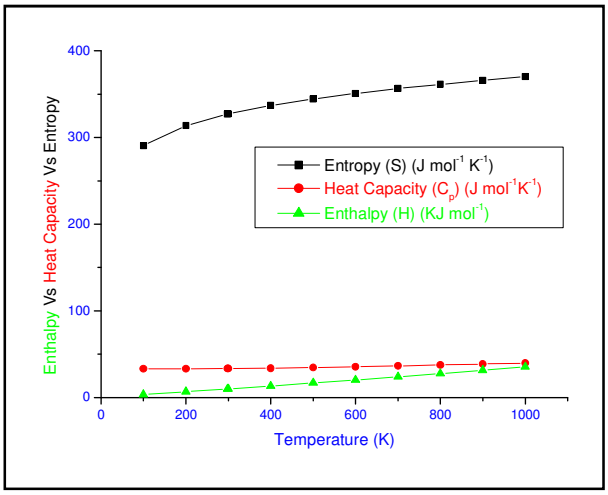

Figure 7: Thermal parameters of DTTP

Bond Length	(Å)	Bond Length	(Å)	Bond Angle	(°)	Bond Angle	(°)	Bond Angle	(°)
N_1-C_2	1.410	C_{18}-C_{20}	1.383	C_2-N_1-C_6	127.891	C_3-C_9-N_{14}	108.202	O_8-C_{18}-C_{20}	141.147
N_1-C_6	1.380	C_{18}-H_{21}	1.083	C_2-N_1-H_7	116.242	C_3-C_9-C_{17}	113.455	C_{17}-C_{18}-C_{20}	118.682
N_1-H_7	1.012	C_{19}-C_{22}	1.389	C_6-N_1-H_7	115.855	C_3-C_9-H_{29}	107.600	C_{20}-C_{18}-H_{21}	119.999
C_2-C_3	1.446	C_{19}-H_{23}	1.084	N_1-C_2-C_3	114.298	N_{14}-C_9-C_{17}	112.136	C_{17}-C_{19}-C_{22}	120.012
C_2-O_8	1.225	C_{20}-C_{24}	1.397	N_1-C_2-O_8	120.023	N_{14}-C_9-H_{29}	107.467	C_{17}-C_{19}-H_{23}	122.151
C_3-C_4	1.361	C_{20}-F_{25}	1.359	C_3-C_2-O_8	125.677	C_{17}-C_9-H_{29}	107.719	C_{22}-C_{19}-H_{23}	117.829
C_3-C_9	1.512	C_{22}-C_{24}	1.396	C_2-C_3-C_4	119.558	C_4-N_{10}-C_{13}	122.605	C_{18}-C_{20}-C_{24}	123.478
C_4-N_5	1.375	C_{22}-F_{26}	1.344	C_2-C_3-C_9	120.464	C_4-N_{10}-H_{15}	121.742	C_{18}-C_{20}-F_{25}	120.763
C_4-N_{10}	1.378	C_{24}-O_{27}	1.356	C_4-C_3-C_9	119.975	N_{10}-C_{13}-N_{14}	114.936	C_{24}-C_{20}-F_{25}	115.7572
N_5-C_6	1.400	O_{27}-H_{28}	0.968	C_3-C_4-N_5	121.678	N_{10}-C_{13}-S_{16}	120.371	C_{19}-C_{22}-C_{24}	121.891
N_5-H_{11}	1.010	C_{13}-N_{14}	1.350	C_3-C_4-N_{10}	120.908	C_9-N_{14}-C_{13}	126.425	C_{24}-C_{22}-F_{26}	118.246
C_6-O_{12}	1.214	C_{13}-S_{16}	1.669	C_4-N_5-C_6	123.467	C_9-N_{14}-H_{30}	117.506	C_{19}-C_{22}-F_{26}	119.8607
C_9-N_{14}	1.471	N_{14}-H_{30}	1.011	C_4-N_5-H_{11}	121.930	C_{13}-N_{14}-H_{30}	113.924	C_{20}-C_{24}-O_{27}	122.725
C_9-C_{17}	1.533	C_{17}-C_{18}	1.401	C_6-N_5-H_{11}	114.498	C_9-C_{17}-C_{18}	118.920	C_{24}-O_{27}-H_{28}	107.453
C_9-H_{29}	1.095	C_{17}-C_{19}	1.399	N_1-C_6-N_5	113.024	C_{18}-C_{17}-C_{19}	119.465	C_{20}-C_{24}-C_{22}	116.468
N_{10}-C_{13}	1.389	N_{10}-H_{15}	1.010	N_5-C_6-O_{12}	122.069	O_8-C_{18}-C_{17}	88.914	C_{22}-C_{24}-O_{27}	120.8053

Table 1: The geometrical parameters of DTTP

Atoms	Charge (a.u)	Atoms	Charge (a.u)
1N	-0.614	16S	-0.254
2C	0.607	17C	0.104
3C	-0.012	18C	-0.170
4C	0.606	19C	-0.186
5N	-0.658	20C	0.317
6C	0.751	21H	0.140
7H	0.296	22C	0.334
8O	-0.518	23H	0.118
9C	-0.045	24C	0.223
10N	-0.608	25F	-0.306
11H	0.288	26F	-0.280
12O	-0.486	27O	-0.542
13C	0.330	28H	0.331
14N	-0.504	29H	0.149
15H	0.289	30H	0.298

Table 2: The Mulliken atomic charges of DTTP

Orbitals	Orbital energies (a.u)	Orbital energies (e.V)
O_{79}	-0.2595	-7.0636
O_{80}	-0.2555	-6.9547
O_{81}	-0.2448	-6.6625
O_{82}	-0.2359	-6.4217
O_{83}	-0.2320	-6.3136
V_{84}	-0.0662	-1.8019
V_{85}	-0.0179	-0.4881
V_{86}	-0.0136	-0.3725
V_{87}	-0.0063	-0.1727
V_{88}	-0.0001	-0.0043

Table 3: Frontier molecular orbitals of DTTP
O-Occupied orbital
V-Virtual orbital

Global reactivity descriptors	Values (eV)
HOMO	-6.3139
LUMO	-1.8019
energy gap (ΔE) = HOMO–LUMO	4.5117
ionization energy $I = -E_{HOMO}$	6.3136
electron affinity $A = -E_{LUMO}$	1.8019
Global hardness (η)= $1/2(E_{LUMO} - E_{HOMO})$	2.2558
Global softness (s) = $S = 1/2\eta$	0.2216
Electro negativity (χ) = $-1/2(E_{LUMO} + E_{HOMO})$	4.0579
Chemical potential (μ) = $-\chi$	-4.0579
global electrophilicity index (Ψ) = $\mu^2/2\eta$	7.2989

Table 4: Global reactivity descriptors of DTTP

Parameters	B3LYP/6-31G(d,p)
Dipole moment (μ)	Debye
μ_x	-0.2153
μ_y	0.3525
μ_z	-0.3613
μ	**0.5487 Debye**
Polarizability (α_0)	x10^{-30}*esu*
α_{xx}	230.55
α_{xy}	-12.24
α_{yy}	136.98
α_{xz}	1.42
α_{yz}	-35.04
α_{zz}	169.85
α	**0.4241 x10^{-30}*esu***
Hyperpolarizability (β_0)	x10^{-30}*esu*
β_{xxx}	59.50
β_{xxy}	291.50
β_{xyy}	43.43
β_{yyy}	209.41
β_{xxz}	-479.79
β_{xyz}	88.37
β_{yyz}	-124.82
β_{xzz}	-147.54
β_{yzz}	107.26
β_{zzz}	137.29
β_0	**6.637x10^{-30}*esu***

Table 5: The molecular electric dipole moments μ (Debye), Polarizability (α_0) and hyperpolarizability (β_0) values of DTTP
*Standard value for urea (μ=1.3732 Debye, β_0=0.3728x10^{-30}esu): **esu**-electrostatic unit*

- Supporting Information

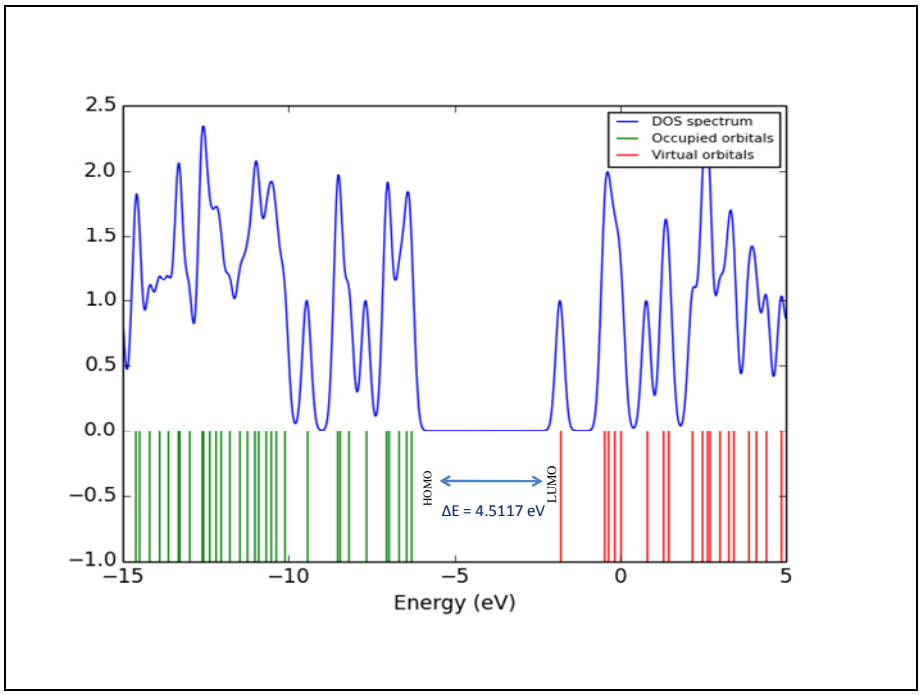

Figure S1: Density of states (DOS) Spectrum of DTTP

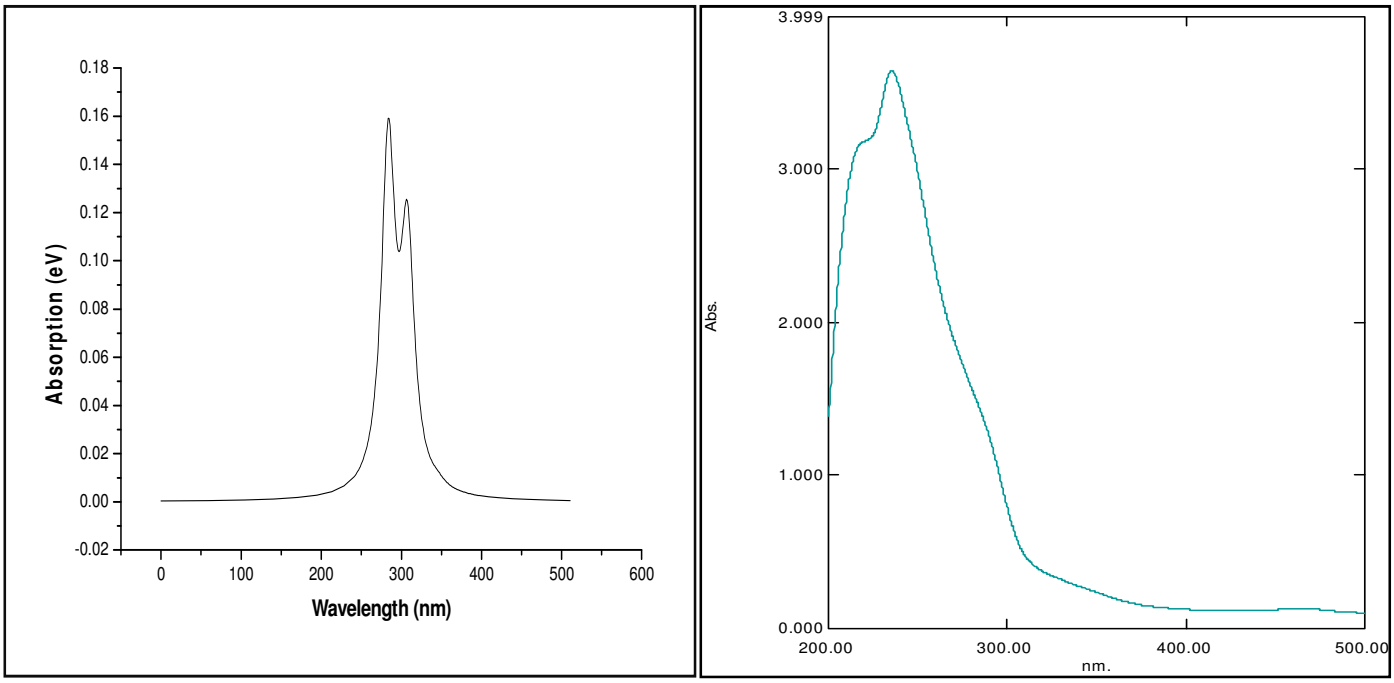

Figure S2: Theoretical and experimental UV spectrum of DTTP

Mode no.	Calculated Frequencies (cm^{-1})		Observed frequencies (cm^{-1})		Intensity		Red mass	Force constant	Assignments[d] PED≥10%
	unscaled	Scaled[a]	FT-IR	FT-Raman	IR[b]	Raman[c]			
1	3793	3644	3734 w		14.32	2.45	1.07	9.03	νO27H28(100)
2	3638	3495			15.82	2.75	1.08	8.41	νN5H11(95)
3	3633	3491	3365vw		3.19	1.27	1.08	8.39	νN10H15(85)
4	3627	3485	3265vw		9.74	0.63	1.08	8.34	νN14H30(92)
5	3624	3482			13.08	2.23	1.08	8.34	νN1H7(100)
6	3232	3105			0.90	1.63	1.09	6.72	νC18H21(100)
7	3223	3097		3069w	0.17	1.26	1.09	6.68	νC19H23(100)
8	3067	2947	2964 w		0.97	2.98	1.09	6.02	νC9H29(99)
9	1851	1778		1767w	100.00	2.56	8.61	17.38	νC6O12(75)
10	1774	1704	1697 m	1680w	65.69	9.43	9.54	17.68	νC2O8(80)
11	1706	1639		1619m	37.22	12.21	7.51	12.87	νC4C3(62)
12	1680	1614	1616 w		0.52	17.16	8.54	14.20	νC18C20(25)+νC19C22(20)+βC22C24C20(15)
13	1663	1598			10.17	0.62	6.46	10.53	νC22C24(28)+νC24C20(15)+νC17C19(20)
14	1596	1533	1523 m		90.11	2.32	2.63	3.94	νC13N14(22)+νC4N10(10)+βH15N10C13(30)+βH30N14C13(18)
15	1565	1504			38.83	0.08	5.14	7.41	νC22C24(10)+νC24C20(22)+νC17C18(15)+νC24O27(15)+βH21C18C20(12)
16	1552	1491			35.22	6.09	3.38	4.80	νC4N5(25)+βH11N5C4(20)+βH30N14C13(15)
17	1496	1437			15.33	0.31	4.37	5.76	νC18C20(20)+νC19C22(22)
18	1460	1403	1400 m		8.74	1.25	2.54	3.19	νC13N14(12)+νC13N10(14)+βH15N10C13(20)+ΓC9C17N14H29(10)
19	1434	1378		1383vw	15.42	1.28	4.19	5.08	νC6N1(14)+νC6N5(10)+βH11N5C4(12)
20	1416	1360			5.19	0.92	1.93	2.28	βH30N14C13(35)
21	1408	1353			4.59	1.41	2.51	2.93	νC18C20(10)+νC17C19(20)+βH28O27C24(16)+βH30N14C13(12)
22	1394	1339	1334 m	1336w	3.73	1.17	1.68	1.92	βH7N1C6(65)
23	1367	1313			23.73	2.82	3.97	4.37	νC19C22(12)+νC17C18(16)+νC22F26(12)+βH29C9C17(15)
24	1342	1289			4.08	3.08	1.48	1.58	βH28O27C24(14)+βH29C9C17(52)
25	1328	1276		1276vw	4.69	0.92	2.71	2.82	ΓC9C17N14H29(40)
26	1299	1248		1244vw	6.07	1.78	3.31	3.29	νC24O27(22)
27	1296	1245			4.55	5.07	2.49	2.47	βH11N5C4(25)
28	1274	1224	1226 m		23.34	0.17	2.54	2.43	νC24O27(18)+βH28O27C24(25)+βH21C18C20(10)
29	1255	1206			9.09	0.42	2.79	2.59	νC4N10(25)+νC2C3(12)+βH15N10C13(15)
30	1241	1192		1194vw	4.40	0.64	1.42	1.29	βH21C18C20(28)+βH23C19C22(38)
31	1223	1175			4.80	0.92	2.69	2.37	νC4N5(16)+νC3C9(12)+ΓC9C17N14H29(25)
32	1153	1108	1126 w		40.38	1.27	2.64	2.07	νC13N10(22)+νC13S16(16)
33	1146	1101			5.44	2.91	1.91	1.48	νC17C9(18)+βH21C18C20(20)+βH23C19C22(18)
34	1124	1080	1072vw	1093m	1.10	1.56	3.00	2.24	νC2N1(20)
35	1054	1013	1020vw		4.54	1.93	5.05	3.30	νC9N14(36)+νC13S16(16)
36	1035	994		989w	12.23	0.45	4.37	2.76	νC22F26(22)+νC20F25(20)
37	1018	978			3.45	0.46	2.90	1.77	νC6N1(12)+νC6N5(28)
38	979	941	954vw		1.23	0.34	5.82	3.29	νC20F25(14)+νC17C9(25)+βC19C22C24(12)
39	948	911			1.53	0.32	4.58	2.42	νC13N10(10)+νC6N5(18)+βC9N14C13(15)
40	887	852	862vs		1.66	1.82	1.35	0.63	τH21C18C20F25(66)+τH23C19C22F26(20)t
41	869	835		813vw	3.01	0.83	1.46	0.65	τH21C18C20F25(12)+τH23C19C22F26(60)
42	823	791	806vs		1.82	8.73	5.58	2.22	νC22C24(12)+νC24C20(14)+νC24O27(20)+βC24C20C18(10)
43	807	775	769m		1.42	3.50	4.02	1.54	ΓC17C3N14C9(20)
44	760	730		733s	5.19	4.37	8.98	3.06	ΓO8C3N1C2(45)
45	741	712	719m		7.71	0.16	10.05	3.25	ΓO12N5N1C6(92)
46	735	706			0.47	7.62	6.50	2.07	ΓO8C3N1C2(20)
47	708	680			1.82	2.11	5.81	1.72	νC2C3(15)+νC13S16(12)
48	689	662		655vw	5.46	2.44	2.30	0.64	τH7N1C2C3(12)+ΓN5C3N10C4(30)
49	668	642			8.03	2.18	4.17	1.10	τC17C19C24C22(14)+ΓN5C3N10C4(10)
50	652	626			3.27	4.85	5.80	1.45	βN1C6O12(12)+βC3C2O8(10)+τC17C19C24C22(15)
51	645	620			1.25	5.57	1.98	0.49	τH7N1C2C3(44)+ΓS16N10N14C13(22)
52	639	614			3.25	1.32	5.40	1.30	ΓF26C19C24C22(14)+ΓO27C20C22C24(25)

53	626	601	607w		12.41	1.50	2.15	0.50	τH30N14C13S16(55)+ΓS16N10N14C13(12)
54	613	589		594vw	1.25	3.80	5.05	1.12	ΓS16N10N14C13(38)
55	602	578			2.42	2.92	3.85	0.82	βC24C20C18(16)+τH30N14C13S16(12)
56	595	572			2.12	2.85	3.26	0.68	βC9N14C13(12)+τH30N14C13S16(16)+ΓS16N10N14C13(14)
57	556	534	543m		1.20	2.24	5.42	0.99	ΓF25C18C24C20(34)+ΓF26C19C24C22(28)
58	553	531		532vw	0.31	3.22	6.53	1.18	νC6N1(10)+βN1C2C3(25)+ΓF25C18C24C20(14)+ΓF26C19C24C22(12)
59	529	508	507vw		13.58	3.22	1.45	0.24	τH11N5C6N1(32)+τH15N10C13N14(40)
60	517	497			0.52	3.81	5.35	0.84	νC22F26(12)+βC19C22C24(30)+βC18C20F25(15)
61	496	477	486vw	478m	0.11	4.48	7.48	1.09	βC22C24C20(25)
62	485	466			1.76	2.21	7.11	0.99	τH15N10C13N14(20)
63	432	415			0.80	0.64	1.16	0.13	τH11N5C6N1(54)+τH15N10C13N14(30)
64	426	409		399vw	6.40	5.69	3.79	0.40	νC2N1(10)+βC3C2O8(20)+βC13N10C4(10)+τH28O27C24C20(20)
65	424	407			11.55	4.42	1.41	0.15	τH28O27C24C20(76)
66	373	358			2.03	1.15	9.25	0.76	βN1C6O12(26)+βC6N1C2(12)+βC13N10C4(10)+βN10C13S16(15)
67	367	353			0.16	5.39	6.48	0.51	ΓO27C20C22C24(25)
68	334	321			0.20	8.58	8.84	0.58	ΓO27C20C22C24(15)
69	321	308			0.25	1.19	9.33	0.57	βC22C24C20(20)+βC24C22F26(15)+βC18C20F25(22)
70	296	284			0.20	3.15	10.98	0.56	βC18C20F25(15)+βN10C13S16(10)
71	282	271			0.87	0.31	7.33	0.34	βC22C24O27(60)+βC24C22F26(22)
72	272	261		269vw	0.21	1.02	7.42	0.32	βC17C9N14(20)+βN10C13S16(12)
73	265	255			0.26	5.59	4.97	0.21	τC19C22C20C24(22)+τC20C18C24C22(42)
74	213	205		219vw	0.29	5.45	9.10	0.24	τC3C9C4N10(36)+τC4C3C2N1(10)
75	194	186			0.11	1.60	10.06	0.22	τC17C19C24C22(14)+ΓC9C17C19C18(10)+ΓC2C4C9C3(22)
76	185	178			0.75	2.82	9.63	0.20	βC19C17C9(15)+βC2C3C9(25)
77	169	162			0.33	7.10	9.56	0.16	βC19C17C9(44)+βN10C13S16(10)
78	155	149			0.25	1.66	10.63	0.15	τC6N1C2C3(66)
79	140	135			0.01	1.61	10.15	0.12	τC17C19C24C22(12)+τC19C22C20C24(34)
80	95	91		100s	0.01	3.32	9.66	0.05	τC4C3C2N1(48)+ΓC9C17C19C18(15)
81	68	65		66vs	0.41	13.52	8.91	0.02	τN10C4C13N14(55)+τC9N14N10C13(12)
82	49	47			0.01	53.38	14.53	0.02	τN10C4C13N14(15)+τC9N14N10C13(50)
83	35	34			0.01	100.00	10.21	0.01	ΓC9C17C19C18(30)+ΓC17C3N14C9(22)+ΓC2C4C9C3(20)
84	18	17			0.05	84.16	11.10	0.00	τC3C9C17C19(75)+τC9N14N10C13(10)

Table S1: The experimental and calculated wavenumbers of DTTP using B3LYP/6-31G(d,p) level of basis set.
ν: Stretching, δ: in-plane-bending, Γ: out-of-plane bending, vw: very weak, w: weak, m: medium, s: strong, vs: very strong, aScaling factor: 0.9608,b Relative IR absorption intensities normalized with highest peak absorption equal to 100, c Relative Raman intensities calculated by Equation and normalized to 100. dPotential energy distribution calculated at B3LYP/6-31G(d,p) level.

TD-DFT/B3LYP/6-31G(d,p)					**Experimental λ_{max} (nm)**
Orbitals		**E (eV)**	**Oscillator Strength (f)**	**Wavelength λ_{max} (nm)**	
Excited State: 1	Singlet-A	3.5882	0.0020	345.53	
81 -> 84	0.12204				
82 -> 84	0.62752				
82 -> 87	0.10389				
83 -> 84	0.23307				
Excited State: 2	Singlet-A	4.0315	0.1021	307.54	
81 -> 84	0.20132				
82 -> 84	-0.26772				
83 -> 84	0.60359				
Excited State: 3	Singlet-A	4.3718	0.1430	283.60	235.40
80 -> 84	0.40415				
81 -> 84	0.50027				
83 -> 84	-0.138				

Table S2: Excitation energies and oscillator strength of DTTP

Type	Donor (i)	ED/e	Acceptor (j)	ED/e	$^{a}E^{(2)}$	$^{b}F(i,j)$	$^{c}E(j)–E(i)$
π–π*	$C_2–O_8$	1.9811	$C_2–O_8$	0.3329	4.44	0.37	0.019
			$C_3–C_4$	0.3261	20.5	0.38	0.042
π–π*	$C_3–C_4$	1.8118	$C_2–O_8$	0.3329	111	0.3	0.083
			$C_3–C_4$	0.3261	25.44	0.31	0.040
			$C_9–C_{17}$	0.0452	15.31	0.68	0.046
			$C_9–H_{29}$	0.0224	6.9	0.75	0.033
π–π*	$C_6–O_{12}$	1.9924	$C_6–O_{12}$	0.3517	9.04	0.38	0.028
			$C_4–N_{10}$	0.0335	8.49	1.28	0.046
			$N_{14}–H_{30}$	0.0156	9.54	1.3	0.049
π–π*	$C_{18}–C_{20}$	1.7009	$C_{17}–C_{19}$	0.3975	78.74	0.3	0.069
			$C_{22}–C_{24}$	0.4337	81.34	0.28	0.069
σ–σ*	$C_{20}–F_{25}$	1.9947	$C_{17}–C_{18}$	0.0198	5.65	1.58	0.041
			$C_{22}–C_{24}$	0.0397	7.11	1.54	0.046
π–π*	$C_{22}–C_{24}$	1.6378	$C_{17}–C_{19}$	0.3975	82.68	0.3	0.070
			$C_{18}–C_{20}$	0.3907	87.91	0.3	0.071
σ–σ*	$O_{27}–H_{28}$	1.9869	$C_{22}–C_{24}$	0.0397	24.06	1.27	0.077
n–π*	N_1	1.6530	$C_2–O_8$	0.3329	214.85	0.28	0.108
			$C_6–O_{12}$	0.3517	265.27	0.27	0.117
n–π*	N_5	1.6751	$C_3–C_4$	0.3261	196.48	0.31	0.107
			$C_6–O_{12}$	0.3517	214.18	0.29	0.110
n–σ*	O_8	1.8587	$N_1–C_2$	0.0888	121.63	0.65	0.124
			$C_2–C_3$	0.0586	74.73	0.73	0.104
n–π*	N_{10}	1.6721	$C_3–C_4$	0.3261	185.6	0.31	0.104
			$C_{13}–S_{16}$	0.3116	58.58	0.38	0.065
			$C_{13}–S_{16}$	0.2538	54.27	0.42	0.067
n–σ*	O_{12}	1.8359	$N_1–C_6$	0.0816	111.17	0.68	0.122
			$N_5–C_6$	0.0886	120.79	0.64	0.124
			$C_{13}–S_{16}$	0.3116	109.83	0.36	0.087
			$C_{13}–S_{16}$	0.2538	48.12	0.4	0.061
n–σ*	S_{16}	1.8781	$N_{10}–C_{13}$	0.0630	49.2	0.59	0.075
			$C_{13}–N_{14}$	0.0545	45.61	0.66	0.077
n–σ*	F_{25}	1.9594	$C_{18}–C_{20}$	0.0240	27.2	1	0.072
			$C_{20}–C_{24}$	0.0408	24.89	0.96	0.067
			$O_{27}–H_{28}$	0.0132	6.99	0.86	0.034
n–π*	F_{25}	1.9286	$C_{18}–C_{20}$	0.3907	74.56	0.43	0.086
n–σ*	F_{26}	1.9645	$C_{19}–C_{22}$	0.0233	25.65	0.97	0.069
			$C_{22}–C_{24}$	0.0397	32.84	0.94	0.077
n–π*	F_{26}	1.9175	$C_{22}–C_{24}$	0.4337	82.84	0.41	0.089
n–σ*	O_{27}	1.9767	$C_{20}–C_{24}$	0.0408	28.58	1.14	0.079
n–π*	O_{27}	1.8684	$C_{22}–C_{24}$	0.4337	121.71	0.33	0.095
π*–σ*	$C_3–C_4$	0.3261	$C_9–C_{17}$	0.0452	5.52	0.38	0.046
			$C_{17}–C_{19}$	0.3975	19.33	0.02	0.015
π*–π*	$C_6–O_{12}$	0.3517	$C_2–O_8$	0.3329	5.23	0.01	0.006
			$C_3–C_4$	0.3261	7.99	0.01	0.008
σ*–π*	$C_{13}–S_{16}$	0.3116	$C_{13}–S_{16}$	0.2538	1044.62	0.04	0.168
π*–σ*	$C_{13}–S_{16}$	0.2538	$C_9–N_{14}$	0.0303	7.28	0.2	0.044
π*–σ*	$C_{17}–C_{19}$	0.3975	$C_3–C_9$	0.0282	7.24	0.37	0.049
π*–π*	$C_{22}–C_{24}$	0.4337	$C_{17}–C_{19}$	0.3975	1152.15	0.01	0.083

Table S3: Second order perturbation theory analysis of fock matrix in NBO basis for DTTP.
aE(2) means energy of hyper conjugative interaction (stabilization energy).
bF(i,j) is the fork matrix element between i and j NBO orbitals.
cEnergy difference between donor (i) and acceptor (j) NBO orbitals.

T (K)	S (J/mol.K)	Cp (J/mol.K)	ddH (kJ/mol)
100.00	290.71	33.26	3.33
200.00	313.76	33.26	6.65
298.15	327.06	33.36	9.92
300.00	327.26	33.36	9.98
400.00	336.91	33.78	13.34
500.00	344.52	34.53	16.75
600.00	350.90	35.48	20.25
700.00	356.45	36.52	23.85
800.00	361.40	37.61	27.55
900.00	365.89	38.73	31.37
1000.00	370.03	39.86	35.30

Table S4: Thermal parameters of DTTP